EUROGRAPHICS 2011 / M. Chen and O. Deussen
(Guest Editors)

Volume 30 (2011), Number 2

The Natural 3D Spiral

Gur Harary and Ayellet Tal

Technion – Israel Institute of Technology

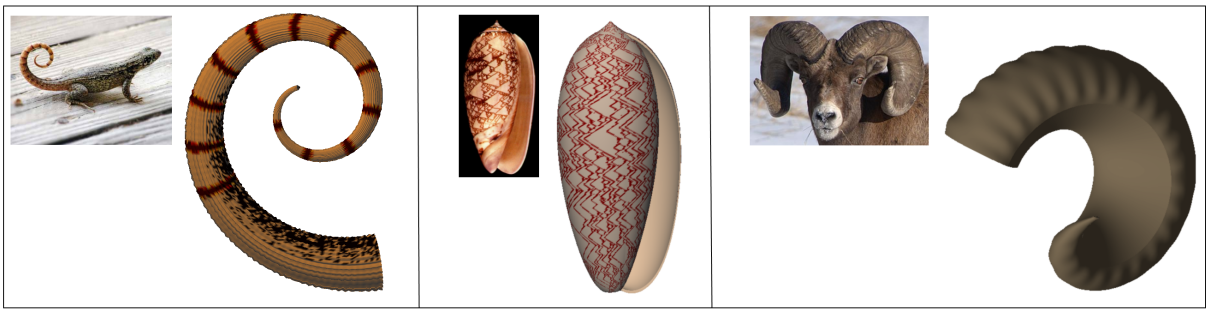

(a) A tail of a lizard (b) Oliva porphyria (c) A horn of a Big-Horn Sheep

Figure 1: *Modeling a variety of logarithmic-spiral structures in fauna. Real images of the objects are shown on the top left.*

Abstract

Logarithmic spirals are ubiquitous in nature. This paper presents a novel mathematical definition of a 3D logarithmic spiral, which provides a proper description of objects found in nature. To motivate our work, we scanned spiral-shaped objects and studied their geometric properties. We consider the extent to which the existing 3D definitions capture these properties. We identify a property that is shared by the objects we investigated and is not satisfied by the existing 3D definitions. This leads us to present our definition in which both the radius of curvature and the radius of torsion change linearly along the curve. We prove that our spiral satisfies several desirable properties, including invariance to similarity transformations, smoothness, symmetry, extensibility, and roundness. Finally, we demonstrate the utility of our curves in the modeling of several animal structures.

Categories and Subject Descriptors (according to ACM CCS): I.3.5 [Computer Graphics]: Computational Geometry and Object Modeling—Curve, surface, solid, and object representations

1. Introduction

Nature is rich in spirals [Coo03, Coo79]. They exist in animal and human anatomy – in horns, seashells, muscles, and bones, as well as in botany – in the formation of leaves, flowers (sunflower heads), fruit (pineapples, pine cones), and tree trunks. Hurricanes are shaped as spirals. Some bays, such as the Half-Moon Bay in California, are spirals. Cook also points to the relation between the incidence of spirals in nature and their appearance in art and architecture.

It is thus not surprising that spirals have attracted the attention of mathematicians as well as biologists, zoologists, paleontologists, artists, and psychologists. In computer graphics, despite the aspiration to produce natural-looking models, relatively few attempts have been made to model spirals. This paper focuses on logarithmic spirals – the ones believed to characterize many of the natural phenomena described above [Mos38, d'A42, Hun70].

The 2D logarithmic spiral is defined in four different manners [d'A42, Hun70]. A few extensions of the 2D logarithmic spiral to 3D were introduced for modeling seashells [Cor89, Pic89, FMP92]. They were demonstrated to produce some beautiful seashells. However, we provide evidence that some of these extensions are too restrictive to describe the richness of spirals in nature, and prove that the other extensions do not hold any 3D definition.

These observations led us to present a different mathematical extension. It requires that both the radius of the curvature and the radius of the torsion change linearly along the curve.

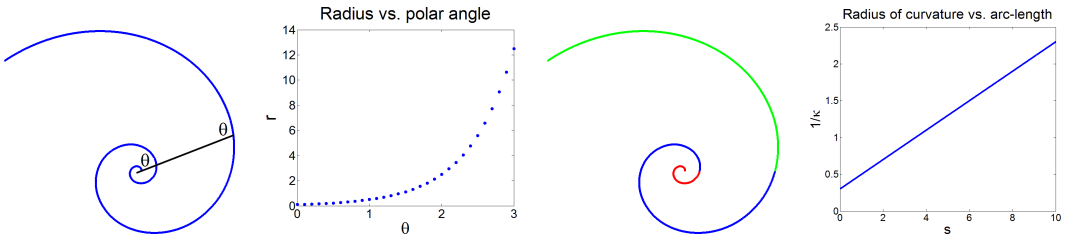

(a) Equiangular spiral (b) Geometrical spiral (c) Proportional spiral (d) Logarithmic spiral

Figure 2: *Different definitions of 2D logarithmic spirals*

To support this definition we show, based on a study of natural objects, that this property indeed characterizes spirals-like objects in nature. In addition, we prove that our spiral satisfies other desirable properties including invariance to similarity transformations, smoothness, symmetry, extensibility (i.e. refinability), and roundness (i.e., if the boundary conditions lie on a circle, the curve is a circle).

We demonstrate the utility of our logarithmic spiral for modeling spiral-shaped animal structures, such as seashells, horns, and tails, as illustrated in Figure 1.

The contribution of this paper is hence threefold. First, we analyze, both theoretically and empirically, some properties of the 3D logarithmic spirals in the literature. We also study characteristics of natural spiral-shaped objects. We show that the two do not conform (Section 3). Second, motivated by the above observation, the paper presents a new extension to 3D of the logarithmic spiral and proves its properties (Section 4). Finally, we demonstrate the utility of our spirals in modeling a variety of natural structures in wildlife (Section 5). We show that the obtained models suit the corresponding natural objects. Altogether, our spirals are evaluated theoretically, empirically, and visually.

2. Background

A variety of spirals have been investigated in computer graphics, including the 3D Helispirals [GS99], Euler spirals [Lev08, HT10], and Logarithmic spirals. This paper focuses on the latter.

2D logarithmic spirals: The planar logarithmic spiral was discovered several times by different mathematicians. The first to discover the spiral was Descartes, who in 1638 named it the *equiangular spiral* after one of its characteristics. Torricelli named it the *geometrical spiral* after another property of the curve – its radius increases exponentially as a function of the angle. Later, Halley named it the *proportional spiral* after its third characteristic. About fifty years later, in 1711, Jacob Bernoulli was the first to describe the curve without using a polar equation. Bernoulli gave the curve its fourth name – the *logarithmic spiral*. He was so fascinated by its mathematical beauty that he also named it *spira mirabilis* (the marvelous spiral) and asked that this curve be engraved on his tombstone. (However, by error, an Archimedean spiral was placed there instead.)

Being discovered by four different mathematicians, each focusing on a different characteristic, the curve can be defined in four different, yet equivalent, ways (see Figure 2):

2D Definition 1 – *Equiangular spiral:* A spiral whose radius vector cuts the curve at a constant angle (Figure 2(a)).

2D Definition 2 – *Geometrical spiral:* A spiral whose radius increases in geometrical progression as its polar angle increases in arithmetical progression: $\theta = t, r = r_0\xi^t$ (Figure 2(b)).

2D Definition 3 – *Proportional spiral:* A spiral in which the lengths of the segments of the curve cut by a fixed radial ray are in continued proportion (Figure 2(c)). In other words, the segments are scaled versions of each other, where the scaling ratios between successive pairs are equal.

2D Definition 4 – *Logarithmic spiral:* A spiral having a linear radius of curvature (i.e., a linear inverse of the curvature): $\kappa(s) = \frac{1}{r_0+\Delta_r s}$ (Figure 2(d)).

3D logarithmic spirals: Extensions of 2D logarithmic spirals to 3D were discussed mostly in the context of modeling seashells. Three different extensions were proposed, all requiring that the projection of the curve onto the xy plane will give a 2D logarithmic spiral.

The first extension requires that $\theta = t,\ r = r_0\xi^t,\ z = z_0\xi^t$, where r_0, z_0 and ξ are constants [Wun67, Cor89, Pic89]. These spirals are known to be paths of one-parameter groups of similarity transformations [Wun67, HOP*05]. In Cartesian coordinates, the spiral is defined as:

$$S_1(t) = [x(t), y(t), z(t)] = \left[r_0\xi^t cos(t), r_0\xi^t sin(t), z_0\xi^t\right]. \quad (1)$$

The second extension is proposed by Pickover [Pic89]. For constants r_0, α, ξ, it is defined as:

$$S_2(t) = [x(t), y(t), z(t)] = [r_0\xi^t cos(t), r_0\xi^t sin(t), \alpha t]. \quad (2)$$

The third extension is presented in [FMP92]. For constants r_0, z_0, ξ_r and ξ_z, the curve is defined as:

$$S_3(t) = [x(t), y(t), z(t)] = [r_0\xi_r^t cos(t), r_0\xi_r^t sin(t), z_0\xi_z^t]. \quad (3)$$

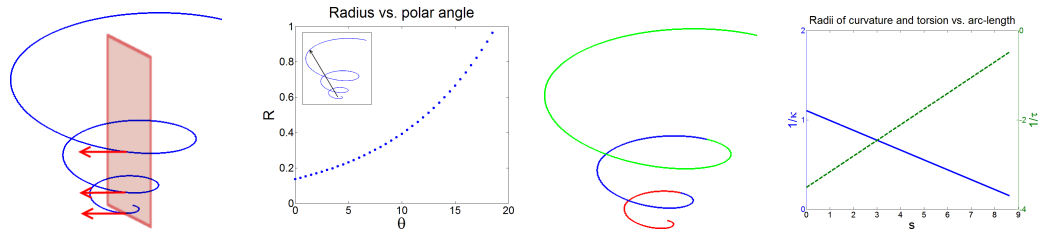

(a) Equitangential spiral (b) Geometrical spiral (c) Proportional spiral (d) Logarithmic spiral

Figure 3: *Different definitions of 3D logarithmic spirals*

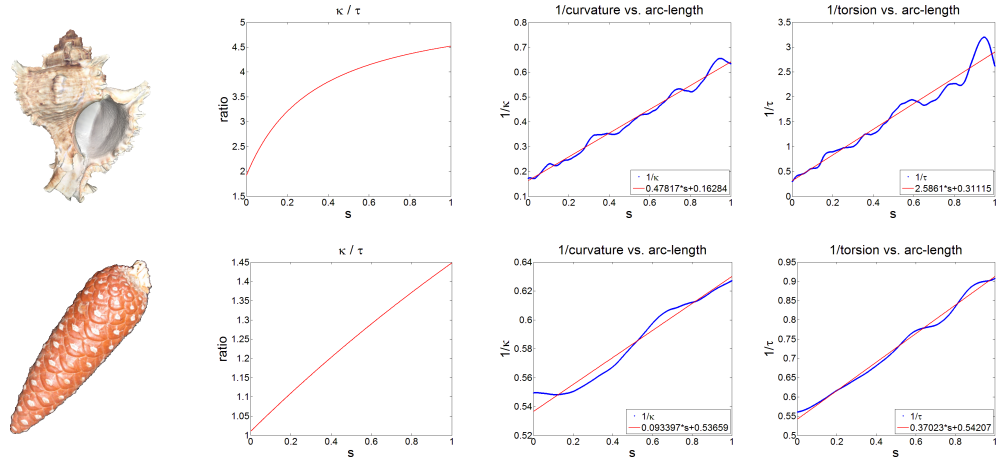

(a) Scanned object (b) Ratio curvature / torsion (c) Linear fit to $1/\kappa$ (d) Linear fit to $1/\tau$

Figure 4: *Two models out of the eleven natural objects we scanned. The ratios between their radii of torsion and their radii of curvature were measured (b). It can be seen that these quantities are not related by scale. The graphs in (c-d) illustrate that the radii of the curvature & torsion, each grows approximately linearly. See additional results in the supplementary material.*

Though this extension generalizes the first extension, in practice, most of the results shown in [FMP92] use a constrained set of parameters ($\xi_r = \xi_z = \xi$), resulting in curves that coincide with those of the first extension.

In the next section we discuss the reasons for the insufficiency of these extensions for modeling some natural logarithmic spiral-shaped objects. In light of this discussion we present in Section 4 a novel definition.

3. Do previous extensions suffice?

We start by giving four definitions of 3D logarithmic spirals, each extends one of the 2D definitions. We then describe our empirical study in which we examine some properties of natural spiral-shaped objects. We consider how well the existing 3D extensions comply with the 3D definitions and whether they suit the properties captured in the study. Finally, we identify a property that is shared by the objects we investigated and is not satisfied by the known extensions.

3D Definition 1 – *Equitangential spiral:* A spiral for which any plane adjacent to the spiral's major axis cuts it at a constant tangent (Figure 3(a)).

3D Definition 2 – *Geometrical spiral:* A spiral for which the length of the radius R increases in geometrical progression as its polar angle θ increases in arithmetical progression, where $R = \sqrt{x^2+y^2+z^2}$ and $\theta = \arctan(y/x)$ (Figure 3(b)).

3D Definition 3 – *Proportional spiral:* A spiral for which the lengths of the segments of the curve, cut by a plane through the spiral's major axis, are in continued proportion (Figure 3(c)).

3D Definition 4 – *Logarithmic spiral:* A spiral having a linear radius of curvature and a linear radius of torsion (Figure 3(d)).

In our study, we scanned eleven seashells, horns, and fruit. Figure 4(a) shows a couple of the scanned objects. We then computed the change in the radius of the curvature ($\frac{1}{\kappa}$) and that of the radius of the torsion ($\frac{1}{\tau}$) for curves on the objects' surfaces. These curves are the smoothed valleys and ridges of the surface. The curvature and the torsion were

computed using the *independent coordinates* method proposed by [LGLC05], which is shown to be robust to noise.

The beauty of the first 3D extension (S_1, Equation (1)) is that it satisfies all four 3D definitions. However, we prove in Appendix A (Proposition A.1) that in this spiral the radius of curvature and the radius of torsion are equal up to a constant (i.e. it is a curve of constant slope). But, our study shows that this is not the case in nature – the radii are not related by any constant; see Figure 4(b). Like any other general 3D curve, the curvature and the torsion are independent. Hence, spirals that relate them are too restrictive and cannot accurately describe the variety of natural spiral objects.

We now turn to examine S_2 and S_3 (Equations (2)–(3)). We prove in Appendix A (Propositions A.2–5) that these spirals do not satisfy any of the above 3D definitions. Hence, while they produce pretty results, theoretically they are not proper extensions. Moreover, we later demonstrate in Figure 6 that these spirals are indeed less accurate for describing natural objects than our spiral.

Finally, our study also shows that linear radii of the curvature and torsion approximately characterize the curves, in accordance with 3D Definition 4; see Figures 4(c-d). This calls for a different mathematical extension of a logarithmic spiral – one that satisfies this definition. This is the rationale behind our definition, which is discussed next.

4. Our 3D logarithmic spiral

The results of the studies presented in Section 3 led us to define a different 3D logarithmic spiral, which generalizes the extension of [Wun67,Cor89,Pic89], yet is able to represent a wider variety of natural objects. This section defines the 3D logarithmic spiral as the curve that satisfies the fourth 3D definition, as illustrated in Figure 5. Obviously, this curve conforms with the definition of the 2D logarithmic spiral. We also prove the curve's existence and uniqueness up to a rigid transformation and some additional properties. Finally, we show that our spiral is more accurate than other logarithmic spirals for approximating real data.

Figure 5: *Our 3D logarithmic spiral*

4.1. Definition & existence

We seek a spiral that has both a linear radius of curvature and a linear radius of torsion in the arc-length parametrization s:

$$\kappa(s) = \frac{1}{(r_0 + \Delta_r s)}, \quad \tau(s) = \frac{1}{(\sigma_0 + \Delta_\sigma s)}, \tag{4}$$

where $r_0, \sigma_0, \Delta_r, \Delta_\sigma$ are constants. Note that curves that satisfy Equation (4) are a special case of the Log-aesthetic curves of [YFS09].

We define the curve that satisfies Equation (4) by a set of differential equations. Assume that we are given the following initial conditions: a point $\mathbf{x}_0$ on the curve, a tangent $\vec{T}_0$ and a normal $\vec{N}_0$ at $\mathbf{x}_0$.

Definition 4.1 The 3D logarithmic spiral is the curve that satisfies the initial conditions for $s = 0$ and the following:

1. $\frac{d\vec{T}(s)}{ds} = \left(\frac{1}{r_0 + \Delta_r s}\right)\vec{N}(s)$,
2. $\frac{d\vec{N}(s)}{ds} = -\left(\frac{1}{r_0 + \Delta_r s}\right)\vec{T}(s) + \left(\frac{1}{\sigma_0 + \Delta_\sigma s}\right)\vec{B}(s)$,
3. $\frac{d\vec{B}(s)}{ds} = -\left(\frac{1}{\sigma_0 + \Delta_\sigma s}\right)\vec{N}(s)$,
4. $|r_0 + \Delta_r s| > 0$ and $|\sigma_0 + \Delta_\sigma s| > 0$.

To understand this definition, observe that 1–3 are the Frenet-Serret Equations [dC76] with our condition for the curvature and the torsion. $\vec{B}$ is the cross product of $\vec{T}$ and $\vec{N}$.

By the definition of the tangent, the spiral $\mathcal{C}(s)$ is:

$$\mathcal{C}(s) = \int_0^s \vec{T}(v)\,dv + \mathbf{x}_0 = \int_0^s \left[\int_0^t \frac{d\vec{T}(u)}{du}\,du + \vec{T}_0\right] dt + \mathbf{x}_0. \tag{5}$$

The following proposition proves the existence of this curve and its uniqueness up to a rigid transformation.

Proposition 4.1 Given constants $r_0, \sigma_0, \Delta_r, \Delta_\sigma, L \in \mathbb{R}$ for which $|r_0 + \Delta_r s| > 0$ and $|\sigma_0 + \Delta_\sigma s| > 0\ \forall s$, $0 \le s \le L$, there exists a 3D logarithmic spiral having linear radii of curvature $\kappa(s) = \frac{1}{(r_0 + \Delta_r s)}$ and torsion $\tau(s) = \frac{1}{(\sigma_0 + \Delta_\sigma s)}$. Moreover, this curve is unique up to a rigid transformation.

Proof By the definition of the curvature of curves in $\mathbb{R}^3$, $\kappa(s) = \left|\frac{d^2\vec{C}}{ds^2}(s)\right| \ge 0$. According to the fundamental theorem of local theory of curves, for every differential function with $\kappa(s) > 0$ and $\tau(s)$, there exists a regular parameterized curve, where $\kappa(s)$ is the curvature, $\tau(s)$ is the torsion, and s is the arc-length parametrization [dC76]. Moreover, any other curve satisfying the same conditions differs by a rigid motion. Note that in our definition $\kappa(s)$ may be negative, and when this happens we consider $|\kappa(s)|$. □

4.2. Properties of the spiral

This section proves that our spiral holds some attractive properties. In [MS92] it is claimed that a curve's fairness is closely related to how little and how smoothly its curvature and its torsion change. Other important properties mentioned in the literature are invariance to similarity transformations, smoothness, symmetry, extensibility, roundness, and being locally constructed [Ull76, Knu79, HT10].
Before, we discussed the smooth change of the curve's curvature and torsion. This section proves that our 3D logarithmic curve also holds the following properties.

1. Invariance to similarity transformations – translation, rotation, and scale. For the latter, we show that scaling of the end-points scales the curve by the same scaling factor.
2. Smoothness: The tangent is defined at every point, i.e., $\frac{\partial \mathcal{C}}{\partial s}$ is finite. (In fact, our curve is C^∞-smooth.)
3. Symmetry: The curve leaving the point $\mathbf{x}_0$ with tangent $\vec{T}_0$ and reaching the point $\mathbf{x}_f$ with tangent $\vec{T}_f$, coincides with the curve leaving the point $\mathbf{x}_f$ with tangent $-\vec{T}_f$ and reaching the point $\mathbf{x}_0$ with tangent $-\vec{T}_0$.
4. Extensibility: For every point $\mathbf{x}_m \in \mathcal{C}$ between the end-points $\mathbf{x}_0$ and $\mathbf{x}_f$, the curves $\mathcal{C}_1$ (between $\mathbf{x}_0$ and $\mathbf{x}_m$) and $\mathcal{C}_2$ (between $\mathbf{x}_m$ and $\mathbf{x}_f$) coincide with $\mathcal{C}$.
5. Roundness: If $\mathcal{C}$ interpolates two point-tangent pairs lying on a circle, then $\mathcal{C}$ is a circle.

Proposition 4.2 A 3D logarithmic spiral is invariant to similarity transformations.

Proof Invariance to rotation and translation results from Proposition 4.1. We next prove scale invariance. We are given a logarithmic spiral $\mathcal{C}$ of length L, which interpolates $\mathbf{x}_0 = \mathcal{C}(0)$ and $\mathbf{x}_f = \mathcal{C}(L)$, and whose parameters are $r_0, \sigma_0, \Delta_r, \Delta_\sigma$. We should show that the spiral $\mathcal{C}_\lambda$, which interpolates $\lambda\mathbf{x}_0$ and $\lambda\mathbf{x}_f$ for $\lambda > 0$, is equal to $\lambda\mathcal{C}$, i.e., $\forall s, 0 \le s \le L \;\; \mathcal{C}_\lambda(s) = \lambda\mathcal{C}(s)$. Thus, we need to find the constants $\widetilde{r_0}, \widetilde{\sigma_0}, \widetilde{\Delta_r}, \widetilde{\Delta_\sigma}, \widetilde{L}$ that define the logarithmic spiral $\mathcal{C}_\lambda$, for which $\mathcal{C}_\lambda(0) = \lambda\mathbf{x}_0$ and $\mathcal{C}_\lambda(\lambda L) = \lambda\mathbf{x}_f$, with tangents $\vec{T}_0$ and $\vec{T}_f$ respectively. Then, we should show that every point on this curve coincides with $\lambda\mathcal{C}$.
It easy to show that the 3D logarithmic spiral having parameters $\widetilde{r_0} = \lambda r_0, \widetilde{\sigma_0} = \lambda\sigma_0, \widetilde{\Delta_r} = \Delta_r, \widetilde{\Delta_\sigma} = \Delta_\sigma, \widetilde{L} = \lambda L$ is the sought-after curve.
This is done by substituting these parameters in Definition 4.1(1–3) and defining a new parameter $v = s/\lambda$ ($\Rightarrow dv = ds/\lambda$). We get that $\frac{d\vec{T}}{ds} = \frac{d\vec{T}}{dv}\frac{dv}{ds} = \frac{1}{\lambda}\frac{d\vec{T}}{dv}$. Similarly, $\frac{d\vec{N}}{ds} = \frac{1}{\lambda}\frac{d\vec{N}}{dv}$ and $\frac{d\vec{B}}{ds} = \frac{1}{\lambda}\frac{d\vec{B}}{dv}$. Hence, this curve satisfies Definition 4.1 with parameter v.
We can now calculate the 3D logarithmic spiral as follows:

$$\begin{aligned}
\vec{T}_\lambda(s) &= \int_0^{\lambda s} \frac{d\vec{T}}{du}du + \vec{T}_0 \\
&\overset{v=u/\lambda}{=} \int_0^{s} \frac{1}{\lambda}\frac{d\vec{T}}{dv}\lambda dv + \vec{T}_0 = \vec{T}(s),
\end{aligned}$$

$$\begin{aligned}
\mathcal{C}_\lambda(s) &= \int_0^{\lambda s}\left[\int_0^{t}\frac{d\vec{T}}{du}du + \vec{T}_0\right]dt + \lambda\mathbf{x}_0 \\
&\overset{v=u/\lambda}{=} \int_0^{\lambda s}\left[\int_0^{t/\lambda}\frac{1}{\lambda}\frac{d\vec{T}}{dv}\lambda dv + \vec{T}_0\right]dt + \lambda\mathbf{x}_0 \\
&\overset{\widehat{t}=t/\lambda}{=} \int_0^{s}\left[\int_0^{\widehat{t}}\frac{d\vec{T}}{dv}dv + \vec{T}_0\right]\lambda d\widehat{t} + \lambda\mathbf{x}_0 = \lambda\mathcal{C}(s).
\end{aligned}$$

This holds for every $0 \le s \le L$. As a special case, we get the boundary conditions $\mathcal{C}_\lambda(0) = \lambda\mathcal{C}(0) = \lambda\mathbf{x}_0$, $\vec{T}_\lambda(0) = \vec{T}(0) = \vec{T}_0$ and $\mathcal{C}_\lambda(\lambda L) = \lambda\mathcal{C}(L) = \lambda\mathbf{x}_f$, $\vec{T}_\lambda(\lambda L) = \vec{T}(L) = \vec{T}_f$. □

Proposition 4.3 A 3D logarithmic spiral is smooth.

Proof According to Proposition 4.1, there exists a solution for the Frenet-Serret equations. Therefore, $\frac{\partial \mathcal{C}}{\partial s} = \vec{T}(s)$ is defined for every $0 \le s \le L$. □

Proposition 4.4 A 3D logarithmic spiral is symmetric.

Proposition 4.5 A 3D logarithmic spiral is extensible.

The proofs of propositions 4.4–4.5 are given in appendix B.

Proposition 4.6 A 3D logarithmic spiral is round.

Proof For given two point-tangent pairs lying on a circle, the circle defined by $r_0 \neq 0, \sigma_0 \to \infty, \Delta_r = 0, \Delta_\sigma = 0$ is a solution of the Frenet-Serret Equations.□

4.3. Results

To verify the suitability of our spiral for describing natural objects, we compared it, as well as the other proposed spirals (S_1, S_2, S_3), to the spirals obtained from our scanned objects (Figure 4). This is done as follows. Given a scanned object, its main axis is found [HOP*05] (this step is needed only for S_2 and S_3). Then, depending on the spiral definition, the values of the free parameter (arc-length s for our spiral and angle t for the other spirals) at sampled points, are found. Next, the alignment between the curves is calculated using [MHTG05]. Finally, the mean-square error (MSE) between the spiral of the scanned object and that of the analytically-computed spiral is computed using a Gradient-Descent algorithm that minimizes this error.
Figure 6 displays some of the results for the normalized objects. It can be seen that our spiral better fits the data than the other spirals and that our error is smaller. We perform comparisons to two out of three previous logarithmic spirals since S_3 includes S_1 as a special case. Thus, in essence, we compared our results to all previous spirals.

S_2	S_3	Our spiral	MSE
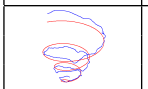	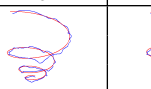		S_2: 5.7E-3 S_3: 1.4E-3 Ours: 0.85E-3
	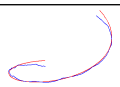	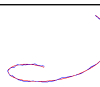	S_2: 0.77E-3 S_3: 1.6E-3 Ours: 0.21E-3

Figure 6: *Fitting the different spirals (red) to the spirals of the real data (blue) in Figure 4(a). Top: seashell, bottom: pine cone. Right: the error obtained by fitting the spirals. See additional results in the supplementary material.*

5. Application: Modeling spiral-like structures in fauna

This section presents our results for modeling seashells, horns, and other animal structures – all believed to comply with the logarithmic structure.

Modeling seashells: The beauty of seashells has attracted the attention of many researchers. Moseley [Mos38] was

the first to characterize seashells with logarithmic spirals. His characteristic was supported experimentally by d'Arcy [d'A42]. Raup [Rau61, Rau62] proposed to model the morphology of a shell. In computer graphics, enhanced appearance of shell models was suggested by [Kaw82, Opp86, PS86]. Increased attention to details was presented in [Ill87, Cor89]. Fowler et al. [FMP92] extended the morphological model of [Cor89] and added a pigmentation pattern to the model, which together resulted in pretty seashells. Our modeling algorithm follows [FMP92]. Therefore, we present it only briefly, for the sake of completeness of the description. The main difference between the algorithms is the use of our spiral to model the seashells instead of S_3. We also address the issue of shell opening, which has not been handled previously.

The algorithm, illustrated in Figure 7, has four steps: First, a 3D logarithmic spiral is constructed. Then, the shell's surface is constructed. Third, the shell's opening is formed, and finally the shell's pattern is generated.

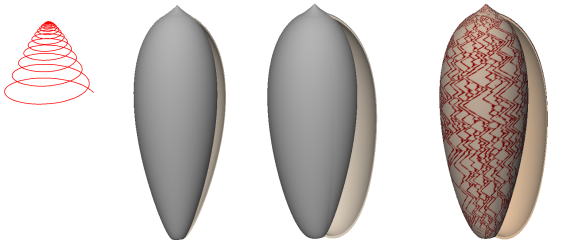

(a) Spiral (b) Surface (c) Opening (d) Pigmentation

Figure 7: *Algorithm outline*

1. 3D LOGARITHMIC SPIRAL CONSTRUCTION: A 3D logarithmic spiral $\mathcal{C}_{log}$ is constructed. This is done by simply choosing the curve's parameters $r_0, \sigma_0, \Delta_r, \Delta_\sigma$ and L, and approximating $\mathcal{C}_{log}$ numerically using the Runge-Kutta 5 (4) method [DP80]. This is an adaptive one-step solver, in which the computation of the point $\mathbf{x}(t_{n+1})$ needs only the solution at the immediately preceding time point $\mathbf{x}(t_n)$. It is designed to produce an estimate of the local truncation error of a single Runge-Kutta step, and as result, allows to control the error with an adaptive step-size. That is done by having two Runge-Kutta methods, one with order 5 and one with order 4. This is to say, the total accumulated error has order h^5 (respectively, h^4), where h is a basic, non-adaptive step-size of t. In practice, we used 250 sample points for the curves in our models. We examined the MSE between these curves and denser curves with 10000 sample points. The average MSE is 1.6E-4.

2. SHELL SURFACE CONSTRUCTION: The surface is built as a general sweep surface, where $\mathcal{C}_{log}$ is the route. In practice, $\mathcal{C}_{log}$ is sampled and a closed curve – *the generating curve* – traverses only the sampled points. The generating curve is scaled along the route linearly w.r.t. the arc-length of the spiral. The resulting surface is represented by a mesh, where a triangle strip is built between every pair of consecutive generating curves.

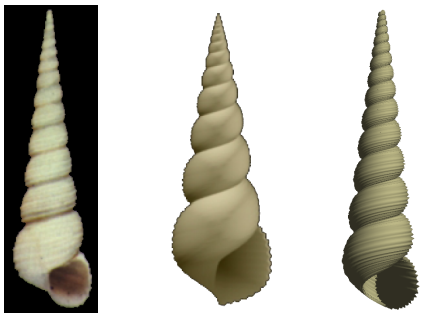

(a) Real seashell (b) [FMP92] (c) Our result

Figure 8: *Turrirella nivea. Our result is similar to the natural Turrirella nivea in width, in the number of revolutions, in the height of each revolution, and in the opening.*

(a) Real seashell (b) [FMP92] (c) Our result

Figure 9: *Papery rapa. Our model captures the general shape as well as the upper tip of the shell and the opening.*

3. FORMING THE SHELL OPENING: The sweeping of a uniformly growing generating curve along the logarithmic spiral produces a strictly self-similar surface that can be mapped onto itself by scale and rotation around the shell axis [d'A42]. In real shells, the lips at the shell opening often display a departure from self-similarity.

We model the opening using a closed curve $\mathcal{C}_{open}$ that describes the shape of the opening. Instead of sweeping the generating curve along the entire logarithmic spiral as done in [FMP92], we sweep it only when the parameter s is in the range $[s_0, L-\Delta L]$. For the rest of the spiral, when $s \in [L-\Delta L, L]$, we use a linear interpolation between the generating curve and $\mathcal{C}_{open}$.

4. PIGMENTATION PATTERN GENERATION: Pigmentation patterns in shells show an enormous amount of diversity. We simulate them using a class of reaction-diffusion models developed by [MK87a, MK87b] and used in [FMP92]. For a given biological model, described by reaction-diffusion differential equations, the solution results in an image, which is mapped to the mesh.

RESULTS: Figures 8–11 illustrate some results obtained by our algorithm. These examples were chosen since they were modeled by [FMP92], and thus they allow us to provide a

(a) Real seashell (b) [FMP92] (c) Our result

Figure 10: *Conus marmoreus. Our spiral yields better modeling of the top and bottom tips, as well as a better opening.*

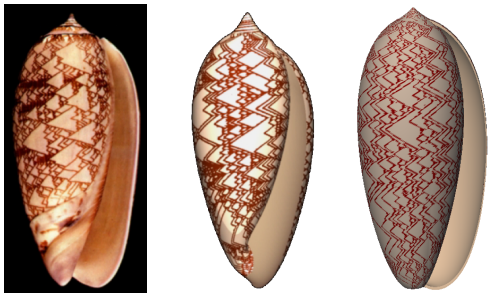

(a) Real seashell (b) [FMP92] (c) Our result

Figure 11: *Oliva porphyria. Note the tips and opening.*

fair comparison to the results presented in their paper as well as to the original images given there. Since the seashells of [FMP92] were produced by a constrained spiral model (S_1 is a special case of S_3), these comparisons can be viewed also as comparisons to S_1.

Our models are more similar to the natural seashells in several manners. First, as our spiral is less restrictive, we are able to produce seashells whose general structure better resembles the natural shells than its competitors (Figures 8–9). Second, the upper and the lower tips of our shells look more natural (Figures 9–10). Finally, since we added opening formation, we are able to control it and produce narrower or wider openings, as required (Figures 10–11). The last two steps of the algorithm – opening formation and pigmentation – were applied only to the models in Figures 10–11.

Modeling horns: Animal horns are structured as logarithmic spirals [d'A42]. Yet, there exist only a few studies that model horns. In [Kaw82, Stę09] a horn is created by assembling given modules along a path. In [Kaw82] every branch of the horn is a 2D spiral, whereas in [Stę09] the path is S_3. We propose to model the geometry of horns in two steps. First, the 3D logarithmic spiral is constructed. Then, a surface that supports *3D texture* (i.e. fluctuations) is constructed, in compliance with the fact that horns have visible 3D textures. We propose to create this structure by adding small fluctuations to the size of the generating curve when traversed along the route $\mathcal{C}_{log}$. The fluctuations can be restricted to only part of the generating curve, as illustrated in Figures 1(c),12,14, where only the "outer" part of the horns has fluctuations.

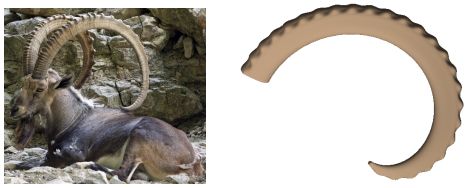

(a) Image of an Ibex (b) Our model

Figure 12: *Horn of an Ibex. Note the outer fluctuations.*

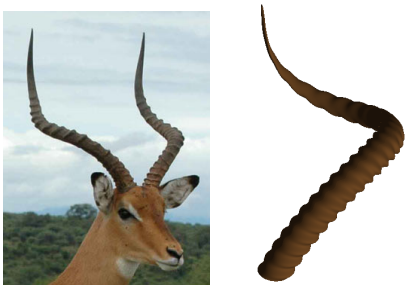

(a) Image of an Impala (b) Our model

Figure 13: *Horn of an Impala. Note the bending of the horn.*

(a) Image of a Kudu (b) [Stę09] (c) Our model

Figure 14: *Horn of a Kudu. Note the twisting.*

The provided results demonstrate not only the 3D fluctuation, but also the ability of our algorithm to support bending (curvature), as demonstrated in Figure 12, and twisting (torsion), shown in Figures 1(c) and 14. Figure 14 also shows the modeling of the Kudu's horn in [Stę09]. (The paper does not provide the image this model is inspired by.)

Modeling other animal structures: A variety of other organs of animals are shaped as logarithmic spirals. Figure 15 shows our model of a cochlea, which is the auditory portion of the inner ear. It is a spiralled, hollow, conical chamber of bone. Figures 1(a) and 16 show our models of spiral-shaped tails – that of a lizard and that of a sea horse. In all these examples, our models resemble the spirals in the images. In Figure 1(a), the mesh was textured using standard texture mapping.

(a) Image of a cochlea (b) Our model

Figure 15: *Cochlea*

(a) Image of a sea horse (b) Our tail model

Figure 16: *Sea horse tail*

Running time and user interaction: The algorithm was implemented in Matlab and ran on a 2Ghz Intel Core 2 Due-processor machine with 2Gb of memory. The running time is about 5 seconds for a 100,000-vertex model.
We built a GUI that allows the user to control the parameters. The user's interaction is similar to that of the previous approaches – requiring to choose a similar number of parameters. Table 1 lists the parameters used for generating the models presented in this paper.

Figure	r_0	Δ_r	σ_0	Δ_σ	L
1(a),11	1	0.2	10	1	57
1(b)	5E-4	0.03	0.1	0.85	0.4
1(c)	0.6	0.1	2	15	5.2
8	0.002	0.025	0.1	0.02	2.6
9	0.008	0.1	10	10	11
10	0.005	0.03	0.2	1.25	5
12	1	0.2	1	1	8
13	0.1	0.5	0.1	1.2	3.5
14	0.01	0.01	3	5	0.12
15	0.005	0.115	0.4	0.4	2.3
16	1.75E-3	0.19	0.2	0.2	0.12

Table 1: *Parameters of the models presented in the paper*

Limitations: Our modeling technique cannot model large spikes and extrusions, which exist in some seashells, e.g., Figure 4 (top). In addition, it cannot handle distortions in the model, such as the one shown at the bottom tip of the shell in Figure 9(a).

6. Conclusion

Logarithmic spirals characterize many natural structures. This paper addressed the challenge of extending the well-known 2D logarithmic spiral to 3D. Our mathematical definition was motivated by studying previous extensions and showing that they may be too restrictive for representing the variety of spiral-shaped objects.
We provide three types of analysis of our spirals as well as of previously proposed spirals: theoretical, empirical, and visual. Theoretically, we prove some desirable properties of the spiral. Empirically, we scanned objects and tested the fit between the mathematical definitions and actual spirals in nature. Visually, we produced models that demonstrate the use of the various spirals for modeling structures that appear in the wildlife. Our spirals outperform the other spirals in all these aspects.

Acknowledgements This research was supported in part by the Israel Science Foundation (ISF) 628/08 and by the Ollendorff Foundation.

References

[Coo03] COOK T.: Spirals in nature and art. *Nature 68* (1903), 296. 1

[Coo79] COOK T.: *The curves of life*. Dover, 1979. 1

[Cor89] CORTIE M.: Models for mollusc shell shape. *South African Journal of Science 85* (1989), 454–460. 1, 2, 4, 6

[d'A42] D'ARCY W.: *On growth and form*. Cambridge Univ. Press, 1942. 1, 6, 7

[dC76] DO CARMO M.: *Differential geometry of curves and surfaces*. Prentice Hall, 1976. 4, 9

[DP80] DORMAND J., PRINCE P.: A family of embedded Runge-Kutta formulae. *Journal of Computational and Applied Mathematics 6*, 1 (1980), 19–26. 6

[FMP92] FOWLER D., MEINHARDT H., PRUSINKIEWICZ P.: Modeling seashells. *ACM Trans. Graph. 26*, 2 (1992), 379–387. 1, 2, 3, 6, 7, 9, 10

[GS99] GLAESER G., STACHEL H.: *Open geometry: OpenGL+ advanced geometry*. Springer Verlag, 1999. 2

[HOP*05] HOFER M., ODEHNAL B., POTTMANN H., STEINER T., WALLNER J.: 3D shape recognition and reconstruction based on line element geometry. In *ICCV* (2005), vol. 2, pp. 1532–1538. 2, 5

[HT10] HARARY G., TAL A.: 3D Euler spirals for 3D curve completion. In *ACM Symp. on Comp. Geometry* (2010). 2, 4

[Hun70] HUNTLEY H.: *The divine proportion: A study in mathematical beauty*. Dover, 1970. 1

[Ill87] ILLERT C.: Formulation and solution of the classical seashell problem. *Il Nuovo Cimento D 9*, 7 (1987), 791–814. 6

[Kaw82] KAWAGUCHI Y.: A morphological study of the form of nature. *SIGGRAPH 16*, 3 (1982), 223–232. 6, 7

[Knu79] KNUTH D.: Mathematical typography. *American Mathematical Society 1*, 2 (1979), 337–372. 4

[Lev08] LEVIEN R.: *The Euler spiral: a mathematical history*. Tech. Rep. UCB/EECS-2008-111, UC, Berkeley, 2008. 2

[LGLC05] LEWINER T., GOMES J., LOPES H., CRAIZER M.: Curvature and torsion estimators based on parametric curve fitting. *Computers & Graphics 29*, 5 (2005), 641–655. 4

[MHTG05] MÜLLER M., HEIDELBERGER B., TESCHNER M., GROSS M.: Meshless deformations based on shape matching. *ACM Trans. on Graphics 24*, 3 (2005), 471–478. 5

[MK87a] MEINHARDT H., KLINGLER M.: A model for pattern formation on the shells of molluscs. *Journal of Theoretical Biology 126*, 63 (1987), 63–89. 6

[MK87b] MEINHARDT H., KLINGLER M.: Pattern formation by coupled oscillations: The pigmentation patterns on the shells of molluscs. *Lecture notes in biomath.*, 71 (1987), 184–198. 6

[Mos38] MOSELEY H.: On the geometrical forms of turbinated and discoid shells. *Philosophical Trans. of the Royal Society of London 128* (1838), 351–370. 1, 5

[MS92] MORETON H., SÉQUIN C.: Functional optimization for fair surface design. *SIGGRAPH 26*, 2 (1992), 167–176. 4

[Opp86] OPPENHEIMER P.: Real time design and animation of fractal plants and trees. *SIGGRAPH 20*, 4 (1986), 55–64. 6

[Pic89] PICKOVER C.: A short recipe for seashell synthesis. *IEEE Comp. Grap. and Applications 9*, 6 (1989), 8–11. 1, 2, 4, 9, 10

[PS86] PRUSINKIEWICZ P., STREIBEL D.: Constraint-based modeling of three-dimensional shapes. In *Graphics Interface* (1986), pp. 158–163. 6

[Rau61] RAUP D.: The geometry of coiling in gastropods. *Proc. of the National Academy of Sciences of the USA 47*, 4 (1961), 602–609. 6

[Rau62] RAUP D.: Computer as aid in describing form in gastropod shells. *Science 138* (1962), 150–152. 6

[Stę09] STĘPIEŃ C.: An IFS-based method for modeling horns, seashells and other natural forms. *Computers & Graphics 33*, 4 (2009), 576–581. 7

[Ull76] ULLMAN S.: Filling-in the gaps: The shape of subjective contours and a model for their generation. *Biological Cybernetics 25*, 1 (1976), 1–6. 4

[Wun67] WUNDERLICH W.: *Darstellende Geometrie*, vol. 2. Bibliographisches Institut, 1967. 2, 4

[YFS09] YOSHIDA N., FUKUDA R., SAITO T.: Log-aesthetic space curve segments. In *SPM* (2009), pp. 35–46. 4

Appendix A: S_1,S_2, S_3 and the 3D definitions

This section discusses the properties of the existing 3D spiral extensions S_1, S_2, S_3 (Equations (1)–(3)).

Proposition A.1 S_1 is a curve of constant slope.

Proof: The curvature and the torsion of the spiral S_1 are calculated as [dC76]:

$$\kappa(t) = \frac{|S_1'(t)\times S_1''(t)|}{|S_1'(t)|^3} = \frac{r_0\sqrt{1+ln^2(\xi)}}{\xi^t[(r_0^2+z_0^2)ln^2(\xi)+r_0^2]},$$

$$\tau(t) = \frac{(S_1'(t)\times S_1''(t))\cdot S_1'''(t)}{|S_1'(t)\times S_1''(t)|^2} = \frac{z_0 ln(\xi)}{\xi^t[(r_0^2+z_0^2)ln^2(\xi)+r_0^2]}.$$

Thus, the spiral has a constant slope:

$$\frac{\tau(t)}{\kappa(t)} = \left(\frac{z_0 ln(\xi)}{r_0\sqrt{1+ln^2(\xi)}}\right). \ \square$$

Hereafter we prove that S_2, S_3 (Equations (2)–(3)) do not satisfy any of the four 3D Definitions. We first prove that 3D Definition 1 is violated in the general case. Then we prove, by providing counter examples, that 3D Definitions 2-4 are violated. In these examples, the parameters used are $r_0 = 1, \alpha = 3, \xi = 1.1$ for S_2 and $r_0 = 1, z_0 = 3, \xi_r = 1.1, \xi_z = 1.5$ for S_3.

Proposition A.2 S_2 and S_3 are not equitangential spirals.

Proof: According to 3D Definition 1, the tangents to the curve at points having polar angles $t_n = t_0 + 2\pi n$ ($n \in \mathbb{N}$) should be equal, thus they should not depend on n.
But, in S_2 the tangent is:

$$\begin{aligned} T_2(t_n) &= [r_0\xi^{t_n}(ln(\xi)cos(t_0) - sin(t_0)), \\ &\quad r_0\xi^{t_n}(ln(\xi)sin(t_0) + cos(t_0)), \alpha]/\|T_2\|, \end{aligned}$$

where $\|T_2\| = \sqrt{r_0^2\xi^{2t_n}(1+ln^2(\xi)) + \alpha^2}$, whereas in S_3 the tangent is:

$$\begin{aligned} T_3(t_n) &= [r_0\xi_r^{t_n}(ln(\xi_r)cos(t_0) - sin(t_0)), \\ &\quad r_0\xi_r^{t_n}(ln(\xi_r)sin(t_0) + cos(t_0)), z_0 ln(\xi_z)\xi_z^{t_n}]/\|T_3\|, \end{aligned}$$

where $\|T_3\| = \sqrt{r_0^2\xi_r^{2t_n}(1+ln^2(\xi_r)) + z_0^2\xi_z^{2t_n}ln^2(\xi_z)}$.
Hence, in both cases the tangents depend on n. $\square$

Proposition A.3 S_2 and S_3 are not geometrical spirals.

Proof: According to 3D Definition 2, the length of the radius should depend exponentially on the polar angle, thus the graph of $log(R)$ w.r.t the polar angle should be linear. Figure 17 demonstrates that for the above counter-examples, the graphs of these spirals are not linear. $\square$

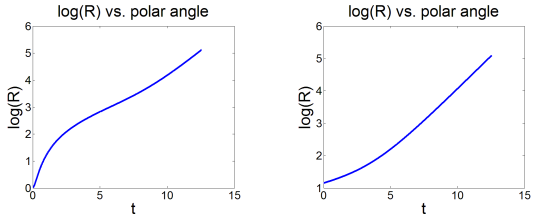

(a) S_2 [Pic89] (b) S_3 [FMP92]

Figure 17: *$log(R)$ vs. t for the parameters specified above*

Proposition A.4 S_2 and S_3 are not proportional spirals.

Proof: According to 3D Definition 3, the ratio between the length of the radii at the polar angles $t_1 = t_0$ and $t_2 = t_0 + 2\pi n$ for $t_0 \in [0, 2\pi]$ and $n \in \mathbb{N}$ should be constant, hence $\frac{R(t_0)}{R(t_0+2\pi n)} = const, \ \forall t_0 \in [0, 2\pi]$.
Figure 18 shows a counter example for $t_0 = 0, \pi/8, \pi/4, 3\pi/8, \pi/2$ and $n = 1$. It shows that in both cases the 3D definition does not hold. $\square$

Proposition A.5 S_2 and S_3 are not logarithmic spirals.

Proof: Figure 19 presents the radius of the curvature and the radius of the torsion for S_2 and S_3 for the counter example

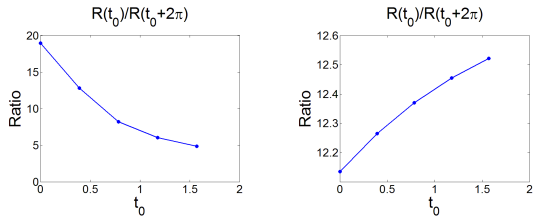

(a) S_2 [Pic89] (b) S_3 [FMP92]

Figure 18: $\frac{R(t_0)}{R(t_0+2\pi)}$ *vs.* t_0

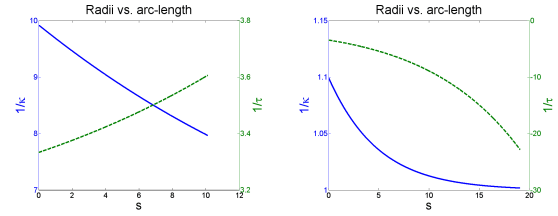

(a) S_2 [Pic89] (b) S_3 [FMP92]

Figure 19: *Radii of the curvature and torsion as a function of s.*

whose parameters are specified above. As can be seen, both do not satisfy 3D Definition 4. □

Appendix B: Proofs of properties of our spiral

Proposition 4.4 A 3D logarithmic spiral is symmetric.

Proof: Given a 3D logarithmic spiral $\mathcal{C}$ that interpolates the point-tangent pairs $(\mathbf{x}_0,\vec{T}_0)$ and $(\mathbf{x}_f,\vec{T}_f)$, we need to show that the 3D logarithmic spiral $\mathcal{C}_{sym}$ that interpolates $(\mathbf{x}_f,-\vec{T}_f)$ and $(\mathbf{x}_0,-\vec{T}_0)$ coincides with $\mathcal{C}$.
Suppose that the parameters of $\mathcal{C}$ are $r_0,\sigma_0,\Delta_r,\Delta_\sigma,L$. We show below that the 3D logarithmic spiral $\mathcal{C}_{sym}$ whose parameters are $\widetilde{r_0}=r_0+\Delta_r L$, $\widetilde{\sigma_0}=\sigma_0+\Delta_\sigma L$, $\widetilde{\Delta_r}=-\Delta_r$, $\widetilde{\Delta_\sigma}=-\Delta_\sigma$, $\widetilde{L}=L$, coincides with $\mathcal{C}$ and that their tangents are opposite. According to Definition 4.1 we get:

$$\begin{aligned}
\frac{d\vec{T}_{\mathcal{C}_{sym}}(s)}{ds} &= \left(\frac{1}{r_0+\Delta_r L-\Delta_r s}\right)\vec{N}_{\mathcal{C}_{sym}}(s),\\
\frac{d\vec{N}_{\mathcal{C}_{sym}}(s)}{ds} &= -\left(\frac{1}{r_0+\Delta_r L-\Delta_r s}\right)\vec{T}_{\mathcal{C}_{sym}}(s)\\
&\quad+\left(\frac{1}{\sigma_0+\Delta_\sigma L-\Delta_\sigma s}\right)\vec{B}_{\mathcal{C}_{sym}}(s),\\
\frac{d\vec{B}_{\mathcal{C}_{sym}}(s)}{ds} &= -\left(\frac{1}{\sigma_0+\Delta_\sigma L-\Delta_\sigma s}\right)\vec{N}_{\mathcal{C}_{sym}}(s).
\end{aligned}$$

By defining a new parameter $v=L-s$ $(\Rightarrow dv=-ds)$, we get that $\frac{d\vec{T}_{\mathcal{C}_{sym}}}{ds}=\frac{d\vec{T}_{\mathcal{C}_{sym}}}{dv}\frac{dv}{ds}=-\frac{d\vec{T}_{\mathcal{C}_{sym}}}{dv}=\frac{d\vec{T}_{\mathcal{C}}}{dv}$. Similarly, $\frac{d\vec{N}_{\mathcal{C}_{sym}}}{ds}=-\frac{d\vec{N}_{\mathcal{C}_{sym}}}{dv}$ and $\frac{d\vec{B}_{\mathcal{C}_{sym}}}{ds}=-\frac{d\vec{B}_{\mathcal{C}_{sym}}}{dv}$. By the tangent definition we get:

$$\begin{aligned}
&\vec{T}_{\mathcal{C}_{sym}}(L-s)=\int_0^{L-s}\frac{d\vec{T}_{\mathcal{C}_{sym}}}{du}du-\vec{T}_f\\
&\overset{v=L-u}{=}\int_L^s\frac{d\vec{T}_{\mathcal{C}_{sym}}}{dv}dv-\vec{T}_f=\int_s^L\frac{d\vec{T}_{\mathcal{C}}}{dv}dv-\left(\int_0^L\frac{d\vec{T}_{\mathcal{C}}}{dv}dv+\vec{T}_0\right)\\
&=-\int_0^s\frac{d\vec{T}_{\mathcal{C}}}{dv}dv-\vec{T}_0=-\vec{T}_{\mathcal{C}}(s).
\end{aligned}$$

We now show that the curve $\mathcal{C}_{sym}$ coincides with the curve $\mathcal{C}$:

$$\begin{aligned}
&\mathcal{C}_{sym}(L-s)=\mathbf{x}_f+\int_0^{L-s}\left[\int_0^t\frac{d\vec{T}_{\mathcal{C}_{sym}}}{du}du-\vec{T}_f\right]dt\\
&\overset{v=L-u}{=}\mathbf{x}_f+\int_0^{L-s}\left[\int_L^{L-t}\frac{d\vec{T}_{\mathcal{C}_{sym}}}{dv}dv-\vec{T}_f\right]dt\\
&\overset{\hat{t}=L-t}{=}\mathbf{x}_f-\int_L^s\left[\int_{\hat{t}}^L\frac{d\vec{T}_{\mathcal{C}}}{dv}dv-\vec{T}_f\right]d\hat{t}\\
&=\mathbf{x}_0+\int_0^s\left[\int_0^{\hat{t}}\frac{d\vec{T}_{\mathcal{C}}}{dv}dv+\vec{T}_0\right]d\hat{t}\overset{Eq.\ (5)}{=}\mathcal{C}(s).\ \square
\end{aligned}$$

Proposition 4.5 A 3D logarithmic spiral is extensible.

Proof: Given a 3D logarithmic spiral $\mathcal{C}$ that interpolates the point-tangent pairs $(\mathbf{x}_0,\vec{T}_0)$ and $(\mathbf{x}_f,\vec{T}_f)$, we will show that for every $(\mathbf{x}_m,\vec{T}_m)$ on $\mathcal{C}$, the curves $\mathcal{C}_1$ between $\mathbf{x}_0$ and $\mathbf{x}_m$ and $\mathcal{C}_2$ between $\mathbf{x}_m$ and $\mathbf{x}_f$ coincide with $\mathcal{C}$.
Assume that $\mathcal{C}$ has parameters $r_0,\sigma_0,\Delta_r,\Delta_\sigma,L$. Let L_1 be the length of the sub-curve of $\mathcal{C}$ from $\mathbf{x}_0$ to $\mathbf{x}_m$. By the tangent definition and by Equation (5):

$$\vec{T}_m=\int_0^{L_1}\frac{d\vec{T}}{du}du+\vec{T}_0, \tag{6}$$

$$\mathbf{x}_m=\int_0^{L_1}\left[\int_0^t\frac{d\vec{T}}{du}du+\vec{T}_0\right]dt+\mathbf{x}_0. \tag{7}$$

By the uniqueness of the curve (Proposition 4.1), $\mathcal{C}_1$ with the parameters $\widehat{r_0}=r_0,\widehat{\sigma_0}=\sigma_0,\widehat{\Delta_r}=\Delta_r,\widehat{\Delta_\sigma}=\Delta_\sigma,\widehat{L}=L_1$, coincides with $\mathcal{C}$ for $0\le s\le L_1$.
Next, we show that $\mathcal{C}_2$ with the parameters $\widetilde{r_0}=r_0+\Delta_r L_1,\widetilde{\sigma_0}=\sigma_0+\Delta_\sigma L_1,\widetilde{\Delta_r}=\Delta_r,\widetilde{\Delta_\sigma}=\Delta_\sigma,\widetilde{L}=L-L_1$, coincides with $\mathcal{C}$ for $L_1\le s\le L$. Let us denote the tangent of the curve $\mathcal{C}$ at $\mathcal{C}(s)$ by $\vec{T}_{\mathcal{C}}(s)$ and the tangent of the curve $\mathcal{C}_2$ at $\mathcal{C}_2(s)$ by $\vec{T}_{\mathcal{C}_2}(s)$. We need to show that $\mathcal{C}_2$ that starts at $(\mathbf{x}_m,\vec{T}_m)$ reaches $\mathcal{C}(s)$ with tangent $\vec{T}_{\mathcal{C}}(s)$, $\forall s, L_1\le s\le L$.
Similarly to the proof of Proposition 4.4, it can be shown that $\forall s, L_1\le s\le L$, the tangent at $\mathcal{C}_2(s-L_1)$ is $\vec{T}_{\mathcal{C}}(s)$:

$$\begin{aligned}
&\vec{T}_{\mathcal{C}_2}(s-L_1)=\int_0^{s-L_1}\frac{d\vec{T}_{\mathcal{C}_2}}{du}du+\vec{T}_m\overset{v=u+L_1}{=}\int_{L_1}^s\frac{d\vec{T}_{\mathcal{C}}}{dv}dv+\vec{T}_m\\
&=\int_{L_1}^s\frac{d\vec{T}_{\mathcal{C}}}{dv}dv+\int_0^{L_1}\frac{d\vec{T}_{\mathcal{C}}}{dv}dv+\vec{T}_0=\int_0^s\frac{d\vec{T}_{\mathcal{C}}}{dv}dv+\vec{T}_0=\vec{T}_{\mathcal{C}}(s).
\end{aligned}$$

Next, we show that $\forall s, L_1\le s\le L$, $\mathcal{C}_2(s-L_1)=\mathcal{C}(s)$:

$$\begin{aligned}
&\mathcal{C}_2(s-L_1)=\mathbf{x}_m+\int_0^{s-L_1}\left[\int_0^t\frac{d\vec{T}_{\mathcal{C}_2}}{du}du+\vec{T}_m\right]dt\\
&\overset{v=u+L_1}{=}\mathbf{x}_m+\int_0^{s-L_1}\left[\int_{L_1}^{t+L_1}\frac{d\vec{T}_{\mathcal{C}}}{dv}dv+\vec{T}_m\right]dt\\
&\overset{\hat{t}=t+L_1}{=}\mathbf{x}_m+\int_{L_1}^s\left[\int_{L_1}^{\hat{t}}\frac{d\vec{T}_{\mathcal{C}}}{dv}dv+\vec{T}_m\right]d\hat{t}\\
&=\mathbf{x}_0+\int_0^{L_1}\left[\int_0^{\hat{t}}\frac{d\vec{T}_{\mathcal{C}}}{dv}dv+\vec{T}_0\right]d\hat{t}+\int_{L_1}^s\left[\int_{L_1}^{\hat{t}}\frac{d\vec{T}_{\mathcal{C}}}{dv}dv+\vec{T}_m\right]d\hat{t}\\
&\overset{Eq.\ (7)}{=}\mathbf{x}_0+\int_0^{L_1}\left[\int_0^{\hat{t}}\frac{d\vec{T}_{\mathcal{C}}}{dv}dv+\vec{T}_0\right]d\hat{t}+\int_{L_1}^s\left[\int_0^{\hat{t}}\frac{d\vec{T}_{\mathcal{C}}}{dv}dv+\vec{T}_0\right]d\hat{t}\\
&\overset{Eq.\ (6)}{=}\mathbf{x}_0+\int_0^s\left[\int_0^{\hat{t}}\frac{d\vec{T}_{\mathcal{C}}}{dv}dv+\vec{T}_0\right]d\hat{t}\overset{Eq.\ (5)}{=}\mathcal{C}(s).\square
\end{aligned}$$